Journal of Materials Chemistry A

Accepted Manuscript

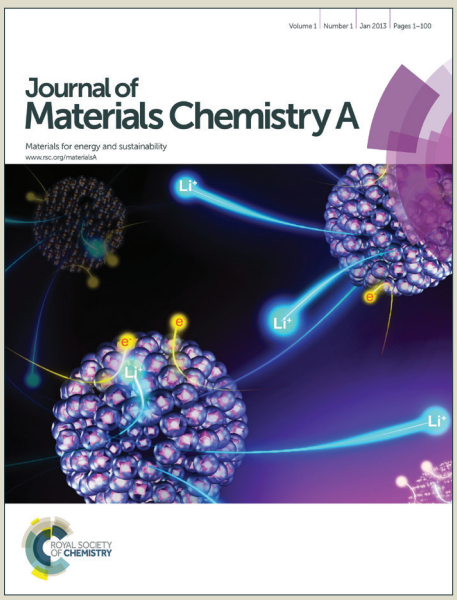

ROYAL SOCIETY OF CHEMISTRY

www.rsc.org/materialsA

Journal of Materials Chemistry A RSCPublishing

ARTICLE

Lithium iron phosphate/nitrogen–doped reduced graphene oxide nanocomposite as a cathode material for high–power lithium ion batteries

Jong-Pil Jegal, Kwang-Chun Kim, Myeong Seong Kim, Kwang-Bum Kim*

Cite this: DOI: 10.1039/x0xx00000x

Received 00th January 2012,
Accepted 00th January 2012

DOI: 10.1039/x0xx00000x

www.rsc.org/

A $LiFePO_4$/nitrogen–doped recued graphene oxide nanocomposite has been synthesized using a solution-based method followed by heat treatment. The nitrogen–doped reduced graphene oxide surrounding the $LiFePO_4$ nanoparticles facilitates the transfer of electrons throughout the electrodes, which significantly reduces the internal resistance of the electrodes, resulting in high utilization of the $LiFePO_4$. Electrodes fabricated with the $LiFePO_4$/nitrogen–doped reduced graphene nanocomposite show high discharge capacities and voltages at high rates including sub–zero temperature conditions, even at commercially acceptable loading levels.

1. Introduction

Because of increasing demands to control CO_2 emissions, the quest for alternative energy sources to replace fossil fuels in automobiles has gained widespread attention.[1,2] For example, hybrid electric vehicles (HEVs) and electric vehicles (EVs) powered by lithium-ion batteries (LIBs) with high energy density have been considered as suitable alternatives to vehicles powered by fossil fuels.[2–4] In this regard, cathode materials with high specific capacities and rate capabilities are in much demand.[2–5] Therefore, many cathode materials with higher capacities than conventional cathode material (i.e., $LiCoO_2$ with a practical capacity of 145 mAh g^{-1}) have been extensively explored, such as $LiNi_xCo_yMn_zO_2$,[6,7] $LiNi_{0.8}Co_{0.15}Al_{0.05}O_2$,[8,9] over-lithiated layered oxides,[10,11] and $Li_xM_y(PO_4)_z$ (M = Fe, Mn, Co, Ni, V).[12–14] Among these, $LiFePO_4$ has been considered as a promising cathode material for LIBs for high–power applications, such as power tools, HEVs and EVs because of its excellent safety, environmental benignity, and high specific capacity (170 mAh g^{-1}).[15,16] However, rate performance of the $LiFePO_4$ is hindered by its poor electrical conductivity (10^{-9} S cm^{-1}) and lithium diffusion rate (10^{-15}–10^{-12} cm^2 s^{-1}).[17,18]

Recent studies on the synthesis of nano-sized $LiFePO_4$ and its decoration with conductive carbon materials, such as amorphous carbon, carbon nanotubes (CNTs), and reduced graphene oxide (rGO), have yielded materials with enhanced rate performance.[19–23] For example, Wu *et al.* synthesized $LiFePO_4$ nanoparticles embedded in a nanoporous carbon matrix, and exhibited a capacity of 40 mAh g^{-1} at a 230 C–rate.[19] Zhou *et al.* fabricated a $LiFePO_4$/graphene composite using a spray-drying technique, and demonstrated a capacity of 70 mAh g^{-1} at a 60 C–rate.[20] In addition, we have previously reported on the synthesis of CNT–embedding $LiFePO_4$, that displayed a capacity of 80 mAh g^{-1} at a 120 C–rate. In this synthesis, urea was used to enhance wettability of the CNTs.[21] Interestingly, urea has also been used as a nitrogen source for doping on carbonaceous materials.[24–26] Such nitrogen-doped carbonaceous materials have exhibited improved electrical conductivity relative to the undoped materials.[24,25,27,28]

In this study, we synthesized a $LiFePO_4$/nitrogen-doped reduced graphene oxide (NrGO) nanocomposite using urea as a nitrogen source and examined its electrochemical performance. The nitrogen was easily doped on reduced graphene oxide (rGO) by using urea as an additive, and the resulting nanocomposite showed low internal resistances, thus fairly good electrochemical performance in terms of the high discharge capacities and voltages at high C–rates including sub–zero temperature conditions. These results demonstrate that the $LiFePO_4$/NrGO nanocomposite has high potential as a cathode material for LIBs for high–power applications.

2. Experimental

2.1 Synthesis of $LiFePO_4$/NrGO nanocomposite

The $LiFePO_4$/NrGO nanocomposite was prepared using a two–step solution-based method. In the first step, a $FePO_4 \cdot H_2O$/NrGO nanocomposite, the precursor for the synthesis of the $LiFePO_4$/NrGO nanocomposite, was synthesized by precipitation method. In specific, graphite oxide powder (0.4 g), prepared by Hummers method, was immersed in a urea solution (1.5 M, 720 ml) (Aldrich) and sonicated in an ice bath for 1 h. Then, a solution of $NH_4H_2PO_4$ (0.75 M, 24 ml)

(Aldrich), and a mixture of $FeSO_4·7H_2O$ (0.75 M, 24 ml) (Aldrich) and citric acid (0.25 M, 8 ml) (Junsei) solutions were added sequentially with vigorous stirring. The solution was heated at 60 °C for 3 h. The product was washed repeatedly with distilled water and acetone, and then dried at 60 °C for 24 h. The as-synthesized $FePO_4·4H_2O$/NrGO nanocomposite was annealed at 300 °C for 6 h in air to obtain the $FePO_4·H_2O$/NrGO nanocomposite. In the second step, $FePO_4·H_2O$/NrGO was chemically lithiated using a 2 M solution of LiI in acetonitrile for 24 h in a glove box filled with Ar. The product was washed with acetone and then dried at 60 °C for 12 h. The dried powder was heat-treated at 700 °C for 3 h in an atmosphere of Ar/H_2 (95:5) to obtain $LiFePO_4$/NrGO nanocomposite.

2.2 Characterization

The structures of the graphite oxide, $FePO_4·H_2O$/NrGO nanocomposite, and $LiFePO_4$/NrGO nanocomposite were characterized by X–ray diffraction (XRD; Rigaku D/MAX 2200V/PC). Data were collected over a 2θ range 5–80°. The morphologies of the $FePO_4·H_2O$/NrGO nanocomposite and the $LiFePO_4$/NrGO nanocomposite were examined by field emission scanning electron microscopy (FE–SEM; Hitachi, S-4300) and transmission electron microscopy (TEM; Philips, CM200). Thermo-gravimetric analysis (TGA; Mettler Toledo, TGA/DSC 1) was performed to determine the loading amount of $LiFePO_4$ in the $LiFePO_4$/NrGO nanocomposite. The analysis was performed in air over temperatures ranging from room temperature to 800 °C, at a heating rate of 10 °C min^{-1}. X–ray photoelectron spectra (XPS, Thermo Scientific K–alpha X–ray photoelectron spectroscopy) were examined to identify the degree of reduction of GO and nitrogen doping.

2.3 Electrochemical measurements

Electrochemical characterization was performed using a coin cell (2032) with a working electrode and a lithium foil as the counter electrode. The working electrode was prepared by mixing 95 wt.% $LiFePO_4$/NrGO nanocomposite and 5 wt.% polyvinylidene fluoride (PVDF; Aldrich), used as a binder, dissolved in *N*–methylpyrrolidone (NMP; Aldrich), without extra conducting agent. The slurry was coated on aluminum foil, dried, and then roll-pressed. The thickness of the electrode was systematically controlled from 10 to 36 μm to examine the effect of the electrode thickness on the electrochemical performance. The densities of the electrodes fabricated with the $LiFePO_4$/NrGO nanocomposite were around 1.5–1.6 g cm^{-3} regardless of the electrode thickness. Galvanostatic charge and discharge tests were performed with C–rates increasing from 0.5 to 20 C in the voltage range 2.0–4.3 V using a potentiostat/galvanostat (MPG2, Bio-logic). A temperature chamber (SU–241, Espec) was used to maintain constant temperatures (25, 0, and −20 °C) for the electrochemical tests. The constant current (CC)/constant voltage (CV) charging method with a current limit of 85 mA/g (0.5 C) was used for the electrochemical tests at 0 and −20 °C. The electrolyte was a 1M $LiPF_6$ dissolved in a mixture of ethyl carbonate (EC) and dimethyl carbonate (DMC) in a volume ratio of 1:1.

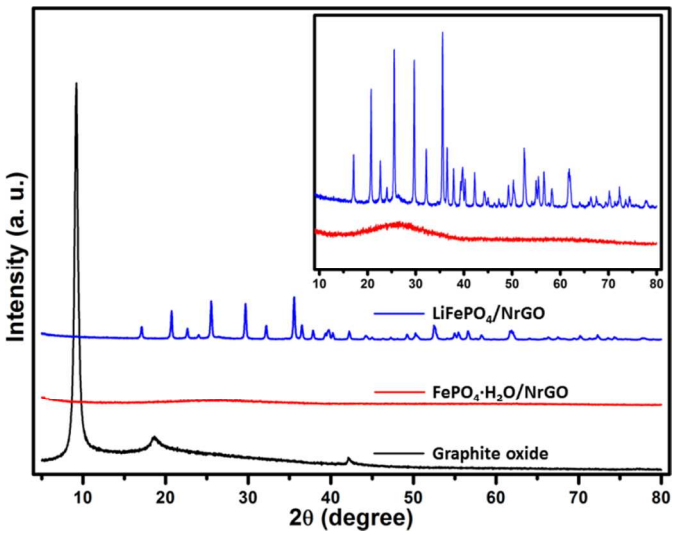

Fig. 1. XRD patterns of graphite oxide, $FePO_4·H_2O$/NrGO nanocomposite, and $LiFePO_4$/NrGO nanocomposite.

3. Results and discussion

Fig. 1 shows the XRD patterns of the graphite oxide, $FePO_4·H_2O$/NrGO, and $LiFePO_4$/NrGO nanocomposites. The most intense peak in the XRD pattern for the graphite oxide occurred at 2θ = 9.2°, corresponding to an inter–layer spacing of around 0.96 nm, which indicated that oxygen–containing functional groups were introduced on the basal plane by the oxidation of graphite using Hummers method.[29] The $FePO_4·H_2O$/NrGO nanocomposite showed only a broad peak around 2θ = 26° (inset), implying that the $FePO_4·H_2O$ in the nanocomposite is amorphous. The amorphous nature of the $FePO_4·H_2O$ is critical to the preparation of stoichiometric $LiFePO_4$, because the amorphous phase of $FePO_4·nH_2O$ shows the maximum reactivity for chemical lithiation.[30] In contrast to the $FePO_4·H_2O$/NrGO nanocomposite, the $LiFePO_4$/NrGO nanocomposite showed sharp diffraction peaks (inset) consistent with a single-phase olivine structure (JCPDS card No. 40-1499). The broad hump near 2θ = 26° is probably due to the presence of NrGO in the nanocomposite.

The SEM image of the $FePO_4·H_2O$/NrGO nanocomposite is shown in Fig. 2a. The $FePO_4·H_2O$/NrGO nanocomposite had a two–dimensional sheet–like shape similar to the graphene oxide (GO). The magnified SEM image (Fig. 2b) showed that the $FePO_4·H_2O$ nanoparticles were uniformly decorated on the NrGO surface. This was achieved by controlling the oxidation rate of the Fe^{2+} ions to suppress the homogeneous nucleation of the $FePO_4·4H_2O$ nanoparticles in the bulk solution, as discussed in our previous work.[31] The $FePO_4·H_2O$ nanoparticles in the nanocomposite are about 20 nm in size, which is much smaller than the sizes of the particles synthesized by simple precipitation method using H_2O_2 as the oxidizing agent, as shown in Fig. S1. The TEM image (Fig. 2c) revealed again that

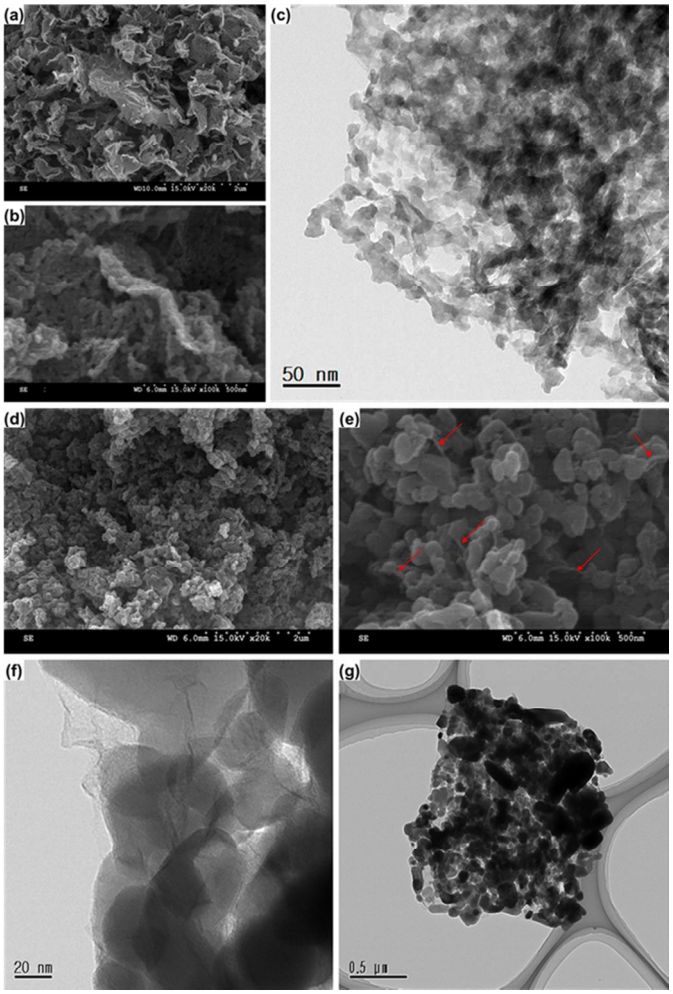

Fig. 2. (a) SEM image, (b) magnified SEM image, (c) TEM image of $FePO_4{\cdot}H_2O$/NrGO, precursor for the synthesis of $LiFePO_4$/NrGO nanocomposite, (d) SEM image, (e) magnified SEM image, (f) magnified TEM image, and (g) low–resolution TEM image of $LiFePO_4$/NrGO nanocomposite.

the $FePO_4{\cdot}H_2O$ nanoparticles were uniformly decorated on the NrGO surface. It should be noted that the $FePO_4{\cdot}H_2O$ in the $FePO_4{\cdot}H_2O$/NrGO is precipitated on the NrGO surface as nanoparticles, whereas the $FePO_4{\cdot}H_2O$ in the $FePO_4{\cdot}H_2O$/CNT reported in our previous work uniformly covers the CNTs in the form of a thin layer.[31] As is known, compared to CNTs, GO has a large number of functional groups on its surface, that act as nucleation sites, which probably leads to the deposition of the $FePO_4{\cdot}H_2O$ as nanoparticles rather than thin layers. The SEM image of the $LiFePO_4$/NrGO (Fig. 2d) showed transformation of the sheet-like $FePO_4{\cdot}H_2O$/NrGO into $LiFePO_4$ nanoparticles incorporated within the NrGO upon lithiation. This could probably be ascribed to the dissolution and re–precipitation, occurring during the chemical lithiation of $FePO_4{\cdot}H_2O$.[21] The presence of NrGO could not be clearly verified from Fig. 2d; however, the high–magnification SEM image (Fig. 2e) revealed the uniform incorporation of the $LiFePO_4$ nanoparticles into the NrGO (which are marked). The exposed NrGO in the nanocomposite can form facile electron conduction pathways throughout the nanocomposite, thus possibly enhance the

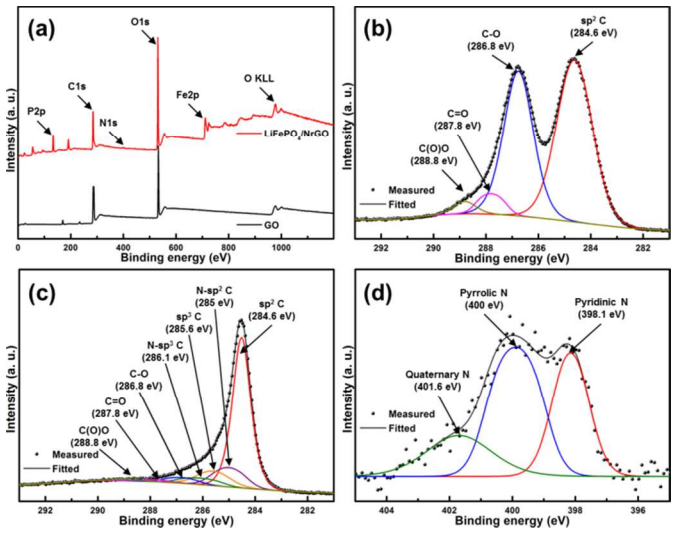

Fig. 3. (a) XPS spectra of graphite oxide and $LiFePO_4$/NrGO nanocomposite, C1*s* XPS spectrum of (b) GO, (c) $LiFePO_4$/NrGO nanocomposite, and (d) N1*s* XPS spectrum of $LiFePO_4$/NrGO nanocomposite.

electrical conductivity of the electrode. The presence of NrGO could be more clearly identified from the TEM image (Fig. 2f). The $LiFePO_4$ nanoparticles were decorated on the surface of the thin wrinkled NrGO layers. The low–resolution TEM image (Fig. 2g) showed that the $LiFePO_4$ nanoparticles that were incorporated within the NrGO layers form micrometer–sized clusters, which makes the handling of the material convenient and enables the fabrication of electrodes with a reduced amount of binder and NMP. The loading amount of $LiFePO_4$ in the $LiFePO_4$/NrGO was determined to be about 88 wt.% by TGA, as shown in Fig. S2.

The degree of reduction of GO and the nitrogen doping achieved during the synthesis of the $LiFePO_4$/NrGO nanocomposite were examined by performing XPS analysis. In the XPS spectrum of the $LiFePO_4$/NrGO (Fig. 3a), Fe2*p* and P2*p* peaks were found while only two strong peaks corresponding to C1*s* and O1*s* were observed for the spectrum of the GO. This change in the XPS spectrum indicates the presence of $LiFePO_4$ in the nanocomposite. The C1*s* peak of the GO (Fig. 3b) could be deconvoluted into four different peaks centered at 284.6, 286.8, 287.8, and 288.8 eV, corresponding to sp^2 C, C–O, C=O, and C(O)O groups, respectively, introduced in the oxidation step. However, the C1*s* XPS spectrum of the $LiFePO_4$/NrGO (Fig. 3c) showed significantly decreased intensities of the C–O, C=O, and C(O)O peaks, demonstrating that the GO was reduced during the synthesis as the nanocomposite underwent heat treatment in a reducing atmosphere to form stoichiometric $LiFePO_4$ with olivine structure. The exact C/O ratio of the NrGO cannot be obtained because of the presence of oxygen in the $LiFePO_4$. However, it is reasonable to say that the high intensity ratio of the sp^2 C peak to the other peaks for oxidized groups is indicative of high degree of reduction of NrGO in the nanocomposite. In addition, the peaks centered at 285 and 286.1 eV in the XPS spectrum revealed the presence of

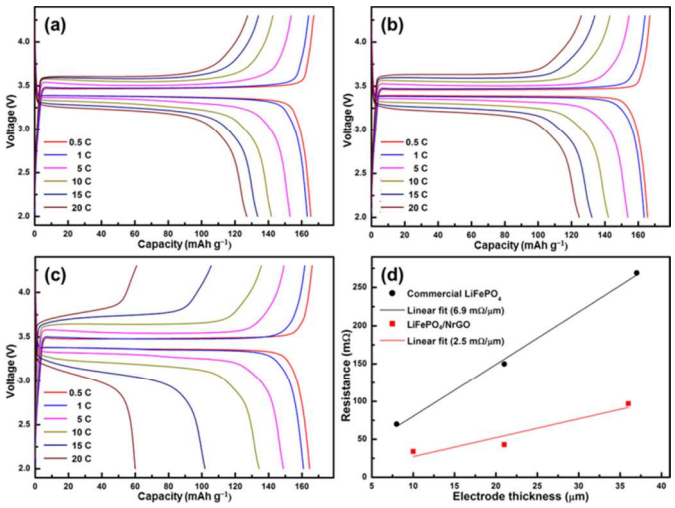

Fig. 4. Charge-discharge profiles of the electrode fabricated with $LiFePO_4$/NrGO nanocomposite at the electrode thickness of (a) 10, (b) 21, (c) 36 μm, and resistance per electrode thickness of the electrodes fabricated with the $LiFePO_4$/NrGO nanocomposite and the commercial $LiFePO_4$.

nitrogen in the nanocomposite and were assigned to N–sp^2 C and N–sp^3 C, respectively.[27,28] The high–resolution N1*s* spectrum of the nanocomposite (Fig. 3d) further confirmed nitrogen doping, in which the peak could be deconvoluted into three different peaks centered at 398.1, 400, and 401.6 eV, corresponding to pyridinic N, pyrrolic N, and quaternary N, respectively.[27,28] The amount of nitrogen in the NrGO is determined to be 2.3 wt.%. These results clearly demonstrate that the nitrogen doping on rGO was achieved by using urea during the synthesis. It has been reported that the doped nitrogen can increase the electrical conductivity of the graphene.[24,25,27,28] Thus, these results suggest the improved rate performance of the $LiFePO_4$/NrGO nanocomposite.

The galvanostatic charge and discharge performance of the $LiFePO_4$/NrGO nanocomposite was evaluated for electrodes of various thicknesses (10, 21, 36 μm) at C–rates from 0.5 to 20 C (Fig. 4). The $LiFePO_4$/NrGO nanocomposite electrode with a thickness of 10 μm showed excellent rate performance up to a 20 C–rate (Fig. 4a). This electrode exhibited an initial discharge capacity of 166 mAh g^{-1} at a 0.5 C–rate based on the weight of $LiFePO_4$ in the nanocomposite and a high discharge capacity of 127 mAh g^{-1} at 20 C–rate, corresponding to 76.5 % of the initial capacity. In addition, the discharge curve at 20 C–rate represented a high discharge plateau over 3.2 V, which is clearly distinguished from the sluggish sloping discharge region. With increase in the electrode thickness to 21 μm, the $LiFePO_4$/NrGO showed little decrease in the discharge capacity (Fig. 4b). The discharge capacity was 125 mAh g^{-1} at a 20 C–rate, corresponding to 75.3 % of the capacity measured at a 0.5 C–rate. Thus, the capacity retention decreased by only 1.2 %, although the electrode thickness was doubled, indicating that the electrode fabricated using the $LiFePO_4$/NrGO has a low internal resistance. When the electrode thickness was further increased to 36 μm, the rate performance of the electrode was diminished (Fig. 4c). The initial capacity at a 0.5 C–rate was 165 mAh g^{-1}, which is comparable to the values obtained from the 10 and 21 μm–thick electrodes. However, the discharge capacity at the 20 C–rate decreased to 60 mAh g^{-1}, which might have been caused by the increase in the internal resistance of the electrode with increasing electrode thickness. However, the high discharge plateau was maintained above 3.0 V up to a 20 C–rate. Moreover, the discharge capacity at a 5 C–rate of the 36 μm–thick electrode was comparable to the values shown by the 10 and 21 μm–thick electrodes. Therefore, these results demonstrate that the electrode fabricated with the $LiFePO_4$/NrGO nanocomposite exhibits reliable rate performance at practical loading levels. In addition, the nanocomposite showed superior rate performance with higher discharge capacities and voltages at given rates compared to the control electrodes fabricated using commercial $LiFePO_4$ with similar electrode thicknesses (Fig. S3). This improved performance may have originated from the lower internal resistance of the electrode fabricated with the $LiFePO_4$/NrGO nanocomposite compared with that of the commercial $LiFePO_4$. In addition, the LiFePO4/NrGO exhibited slightly superior rate performance than $LiFePO_4$/rGO synthesized with the same synthetic method except the addition of urea (Fig. S4), which demonstrates that the nitrogen doping probably enhances the electrical conductivity of the rGO. In order to evaluate the internal resistance of the electrodes quantitatively, initial voltage drop of the electrodes was measured as a function of the electrode thickness. As can be seen in Fig. S5a, the voltage drop of the $LiFePO_4$/NrGO nanocomposite almost linearly increased with the current density, and the slope increases with the electrode thickness. The electrodes fabricated with commercial $LiFePO_4$ showed a similar trend with steeper slope (Fig. S5b). The resulting resistance per electrode thickness value calculated using the slops was 6.9 mΩ/μm for the commercial $LiFePO_4$, while that of the $LiFePO_4$/NrGO was 2.5 mΩ/μm. This value is under half of that exhibited by the commercial $LiFePO_4$ electrodes. The reduced internal resistances could be attributed to high electrical conductivity of the $LiFePO_4$/NrGO nanocomposite caused by the uniform incorporation of highly conductive NrGO and its large surface area, which is sufficient to allow the percolation of the $LiFePO_4$ nanoparticles. By considering the facts that the surface area (33 and 18 m^2 g^{-1} for $LiFePO_4$ in the $LiFePO_4$/NrGO and commercial one, respectively), and the apparent diffusion coefficients (Table S1) of the $LiFePO_4$/NrGO is only slightly higher than the commercial $LiFePO_4$, it is reasonable to say that the uniform incorporation of the NrGO enables the nanocomposite to demonstrate higher effective surface area than the commercial $LiFePO_4$ as well as higher electrical conductivity. This most likely resulted in the superior rate performances of the $LiFePO_4$/NrGO nanocomposite compared to the commercial $LiFePO_4$. These results are also supported by the EIS results shown in Fig. S6. Compared to the commercial $LiFePO_4$, the $LiFePO_4$/NrGO nanocomposite exhibits negligible impedance for the parallel elements and decreased charge transfer resistance because of enhanced electrical conductivity due to the intimate contact between $LiFePO_4$

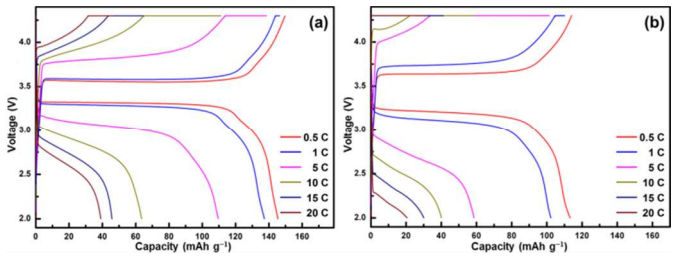

Fig. 5. Charge-discharge profiles of the 36 μm–thick electrodes fabricated with $LiFePO_4$/NrGO nanocomposite at the temperature of (a) 0, and (b) −20 °C.

nanoparticles and highly conductive NrGO.

The low temperature performance of the $LiFePO_4$/NrGO nanocomposite was examined at 0 and −20 °C. Fig. 5a shows the charge and discharge profiles obtained at 0 °C with C–rates from 0.5 to 20 C, for the electrode with a thickness of 36 μm. The electrode exhibited a reduced capacity of 145 mAh g^{-1} along with an increased polarization between the charge and discharge plateaus of 250 mV at a 0.5 C–rate compared to those observed at 25 °C (166 mAh g^{-1}, 116 mV), as shown in Fig. 4c. The decrease in the capacity and increase in the polarization are mainly caused by the decrease in diffusivity of Li^+ ions in the solid $LiFePO_4$.[32] The apparent diffusion coefficients obtained from the cyclic voltammograms (Fig. S5) using the Randle-Sevcik equation[33] clearly demonstrate the decrease in the diffusion coefficient with decreasing temperature (Table S1). However, the electrode fabricated with the $LiFePO_4$/NrGO nanocomposite maintained fairly good rate performances with a high discharge plateaus over 3 V up to a 5 C–rate. As the temperature decreased to −20 °C, the rate performance of the $LiFePO_4$/NrGO obviously deteriorated. The capacity was decreased to 113 mAh g^{-1}, and the polarization increased to 457 mV at a 0.5 C–rate (Fig. 5b). In addition, the discharge plateaus were not clearly distinguished from the sluggish sloping discharge region at C-rates higher than 5 C. However, the electrode could retain a discharge capacity of 102 mAh g^{-1} with a discharge plateau of 3.15 V at 1 C-rate, which is a fairly large capacity compared to reported value obtained at −20 °C.[32] This demonstrates that the diffusion of Li^+ ions in the electrolyte solution and the solid $LiFePO_4$ is critically affected by the operation temperature; however, the electrode fabricated with the $LiFePO_4$/NrGO nanocomposite can sustain a high discharge capacities and voltages because of facile electron transport from/to the $LiFePO_4$ owing to the NrGO surrounding the $LiFePO_4$ nanoparticles.

4. Conclusions

A $LiFePO_4$/NrGO nanocomposite was synthesized using a solution-based method followed by heat treatment. The incorporation of $LiFePO_4$ nanoparticles within NrGO layers enables facile transfer of electrons in the electrode because of the high electrical conductivity of the NrGO and its nanocomposite structure. In result, the $LiFePO_4$/NrGO nanocomposite shows a reduced internal resistance compared to those of electrodes fabricated with the commercial $LiFePO_4$ nanoparticles and carbon black, leading to superior rate performances including sub–zero temperature conditions. In addition, the $LiFePO_4$/NrGO exhibits reliable electrochemical performance even at a commercially acceptable loading level in the electrode.

Acknowledgements

This work was supported by the energy efficiency and resources of the Korea Institute of Energy Technology Evaluation and Planning (KETEP) granted by the Ministry of Knowledge Economy, Korean government (no: 20122010100140).

Notes and references

Department of Materials Science and Engineering, Yonsei University, 134 Shinchon-Dong, Seodaemoon-gu, Seoul 120-749, Republic of Korea. Fax: +82-2-312-5375; Tel: +82-2-365-7745; E-mail:kbkim@yonsei.ac.kr.

Electronic Supplementary Information (ESI) available: SEM image of the $FePO_4 \cdot H_2O$ nanoparticles synthesized by a simple precipitation method using H_2O_2 as the oxidizing agent (Fig. S1), TGA curve of the $LiFePO_4$/NrGO nanocomposite (Fig. S2), charge-discharge profiles of the control electrode fabricated with the commercial $LiFePO_4$ nanoparticles at different electrode thicknesses (Fig. S3), EIS data for the electrodes fabricated with the $LiFePO_4$/NrGO nanocomposite and the commercial $LiFePO_4$ nanoparticles (Fig. S4), cyclic voltammograms of the $LiFePO_4$/NrGO nanocomposite measured at 25, 0, and −20 °C (Fig. S5), and apparent diffusion coefficients of the $LiFePO_4$/NrGO nanocomposite according to the temperatures (Table S1). See DOI: 10.1039/b000000x/

1 D. A. Notter, M. Gauch, R. Widmer, P. Wager, A. Stamp, R. Zah and H. -J. Althaus, *Environ. Sci. Technol.*, 2010, **44**, 6550–6556.
2 B. Scrosati and J. Garche, *J. Power Sources*, 2010, **195**, 2419–2430.
3 M. Armand and J. -M. Tarascon, *Nature*, 2008, **451**, 652–657.
4 K. S. Kang, Y. S. Meng, J. Breger, C. P. Grey and G. Ceder, *Science*, 2006, **311**, 977–980.
5 M. Wakihara, *Mater. Sci. Eng. R*, 2001, **33**, 109–134.
6 K. M. Shaju and P. G. Bruce, *Adv. Mater.*, 2006, **16**, 2330–2334.
7 N. Yabuuchi and T. Ohzuku, *J. Power Sources*, 2003, **119–121**, 171–174.
8 Y. Seino, T. Ota and K. Takada, *J. Power Sources*, 2011, **196**, 6488–6492.
9 D. J. Lee, B. Scrosati and Y. K. Sun, *J. Power Sources*, 2011, **196**, 7742–7746.
10 M. Jiang, B. Key, Y. S. Meng and C. P. Grey, *Chem. Mater.*, 2009, **21**, 2733–2745.
11 J. H. Hong, D. H. Seo, S. W. Kim, H. J. Gwon, S. T. Oh and K. S. Kang, *J. Mater. Chem.*, 2010, **20**, 10179–10186.
12 H. J. Gwon, D. H. Seo, S. W. Kim, J. S. Kim and K. S. Kang, *Adv. Funct. Mater.*, 2009, **19**, 3285–3292.
13 A. V. Murugan, T. Muraliganth, P. J. Ferreira and A. Manthiram, *Inorg. Chem.*, 2009, **48**, 946–952.
14 S. -C. Yin, H. Godney, P. Strobel, M. Anne and L. F. Nazar, *J. Am. Chem. Soc.*, 2003, **125**, 10402–10411.
15 A. K. Padhi, K. S. Nanjundaswamy and J. B. Goodenough, *J. Electrochem. Soc.*, 1997, **144**, 1188–1194.

16 P. Gibot, M. Casas-Cabanas, L. Laffont, S. Levasseur, P. Carlach, S. Hamelet, J. -M. Tarascon and C. Masquelier, *Nature Mater.*, 2008, **7**, 741–747.
17 Z. M. Lou and Y. X. Zhang, *J. Mater. Chem.*, 2011, **21**, 4156–4160.
18 J. W. Fergus, *J. Power Sources*, 2010, **195**, 939–954.
19 X. L. Wu, L. Y. Jiang, F. F. Cao, Y. G. Guo and L. J. Wan, *Adv. Mater.*, 2009, **21**, 2710–2714.
20 J. P. Jegal and K. B. Kim, *J. Power Sources*, 2013, **243**, 859–864.
21 X. F. Zhou, E. Wang, Y. M. Zhu and Z. P. Liu, *J. Mater. Chem.*, 2011, **21**, 3353–3358.
22 Q. Fan, L. X. Lei, X. G. Xu, G. Yin and Y. M. Sun, *J. Power Sources*, 2014, **257**, 65–69.
23 B. Wang, D. L. Wang, Q. M. Wang, T. F. Liu, C. F. Guo and X. S. Zhao, *J. Mater. Chem. A*, 2013, **1**, 135–144.
24 H. L. Guo, P. Su, X. F. Kang and S. K. Ning, *J. Mater. Chem. A*, 2013, **1**, 2248–2255.
25 Z. B. Lei, L. Lu and X. S. Zhao, *Energy Environ. Sci.*, 2012, **5**, 6391–6399.
26 Z. Y. Lin, G. Waller, Y. Liu, M. L. Liu and C. P. Wong, *Adv. Energy Mater.*, 2012, **2**, 884–888.
27 Z. S. Wu, W. Ren, L. Xu, F. Li and H. M. Cheng, *ACS nano*, 2011, **5**, 5463–5471.
28 S. H. Yang, X. F. Song, P. Zhang and L. Gao, *J. Mater. Chem. A*, 2013, **1**, 14162–14169.
29 Y. W. Zhu, S. Murali, M. D. Stoller, A. Velamakanni, R. D. Piner and R. S. Ruoff, *Carbon*, 2010, **48**, 2106–2122.
30 Y. N. Song, S. F. Yang, P. Y. Zavalij and M. S. Whittingham, *Mater. Res. Bull.*, 2002, **37**, 1249–1257.
31 J. P. Jegal, J. G. Kim and K. B. Kim, *Electrochem. Commun.*, 2013, **30**, 87–90.
32 X. Z. Liao, Z. F. Ma, Q. Gong, Y. S. He, L. Pei and L. J. Zeng, *Electrochem. Commun.*, 2008, **10**, 691–694.
33 Y. W. Yu, C. Fietzek, W. Weydanz, K. Donoue, T. Inoue, H. Kurokawa and S. Fujitani, *J. Electrochem. Soc.*, 2007, **154**, A253–A257.